Finite difference modeling of 2D GPR data considering attenuation

Michael Heimer, Marco A. Barsotelli Botelho and Saulo Pomponet Oliveira, UFBA, Brazil

This paper was prepared for presentation at the 9th International Congress of the Brazilian Geophysical Society held in Salvador, Brazil, 11-14 September 2005.

Abstract

We use a finite-difference scheme to simulate 2D ground penetrating radar data by solving the damped wave equation. We show that the stability condition for the damped scalar wave equation does not depend on the damping factor. As an example application of our modeling tool we investigate a typical situation in granite prospecting, where a conductive clay overburden masks the real position of the fractures in the granite. The results of the modeling have a good agreement with the actual data. Also, the algorithm shows well the increase in attenuation with the increase of the frequency. The algorithm shows to be a good basic modeling tool that can be used for further applications and for comparisons with other modeling methods like pseudospectral or finite elements.

Introduction

2D forward numerical modeling of GPR data is an important tool to validate the interpretation of actual radargrams. Goodman (1994) and Cai and McMechan (1995) presented forward modeling routines using ray-tracing techniques. The drawback of these techniques is that they do not simulate diffraction events, as outlined by Zeng et al. (1995), who presented modeling by Fourier methods and compared them with the ray methods. Casper and Kung (1996) applied the pseudospectral forward modeling algorithm on GPR based on an explicit solution of the 2-D lossy electromagnetic wave equation and Chen and Huang (1996) used finite-differences following the same approach.

All these methods have in common the assumption of a dielectric behavior of the earth, which is valid for most geologic applications of GPR, figuring in the frequency range between 10 and 1000 MHz, and imaging materials with conductivities lower than 100 mS/m (Davis and Annan, 1989).

Under such conditions the velocity of propagation remains constant and the attenuation may be considered seperately from the velocity, what gives the electromagnetic radar waves the same behavior as the seismic acoustic waves.

In the present work we use this electromagnetic-acoustic analogy and employ classical finite-differences to solve the damped scalar wave equation following Chen and Huang (1996) and Alford et. al. (1974). We show that the stability condition for the damped scalar wave equation does not depend on the damping factor, therefore reducing to the same condition presented by Alford et. al. (1974) for the wave equation without attenuation. Also, we study the effect of attenuation on radargrams by computing 2D synthetic zero-offset sections.

As an example application of our modeling tool we investigate a typical situation in granite prospecting, where a conductive clay overburden masks the real position of the fractures in the granite. The results of the modeling have a good agreement with the actual data and show the usefulness of our approach.

The algorithm shows to be a good basic modeling tool that can be used for further applications in migration or for comparisons with other modeling methods like the pseudospectral or finite elements.

The Electromagnetic Wave Equation

Our derivation of the 2D electromagnetic damped wave-equation follows Casper and Kung (1996).

Maxwell's equations are

$$\nabla \times \mathbf{E} = -\frac{\partial \mathbf{B}}{\partial t} - \mathbf{M_s} \quad (1)$$

$$\nabla \times \mathbf{H} = \frac{\partial \mathbf{D}}{\partial t} + \mathbf{J_c} + \mathbf{J_s} \quad (2)$$

$$\nabla \cdot \mathbf{D} = q_v \quad (3)$$

$$\nabla \cdot \mathbf{B} = 0 \quad (4)$$

where **E** is the electric field intensity (V/m), **D** is the electric flux density (C/m^2), **H** is the magnetic field intensity (A/m), **B** is the magnetic flux density W/m^2, $\mathbf{J_c}$ is the electrical current density (A/m^2), $\mathbf{J_s}$ is the electric source current density (A/m^2), $\mathbf{M_s}$ is the magnetic source current density (V/m^2) and q_v is the electrical charge density (C/m^3). Note that all these quantities are functions of position and time.

We employ the constitutive relations for linear and isotropic media:

$$\mathbf{D} = \varepsilon \mathbf{E} \quad (5)$$

$$\mathbf{B} = \mu \mathbf{H} \quad (6)$$

$$\mathbf{J} = \sigma \mathbf{E} \quad (7)$$

where ε is the electrical permitivity (F/m), μ the magnetic permeability (H/m) and σ the electrical conductivity (S/m) of the medium, all of them time invariant.

We make the following assumptions:

- σ and ε depend on x and z
- **E**, **D**, **H** and **B** depend on x, z and t
- $\mu = \mu_0$
- $\mathbf{J_c} = 0$ and $q_v = 0$

In two dimensions there are two independent orthogonal polarizations of the electric and the magnetic field components: the transverse electric (TE) mode with field components E_y, H_x H_z and the transverse magnetic (TM) mode with field components H_y, E_x, E_z. We simulate the GPR system antenna as an infinite current line oriented along the y-axis, what yields the radiation in the TE mode.

Under this assumptions, the vector wave equation for the electric field is reduced to the damped scalar wave-equation (Casper and Kung 1996):

$$\frac{\partial^2 \mathbf{E_y}}{\partial t^2} - \frac{1}{\mu_0 \varepsilon(x,z)} \nabla^2 \mathbf{E_y} + \frac{\sigma(x,z)}{\varepsilon(x,z)} \frac{\partial \mathbf{E_y}}{\partial t} = 0 \qquad (8)$$

The finite-difference scheme

We solve the equation (8) following the scheme proposed by Alford et al. (1974) for seismic waves with finite-differences operators of fourth order to discretize the spatial derivatives and with finite-differences operators of second order in time. The time derivative of the atenuation term is solved with a centered difference operator of second order

$$\frac{\partial \mathbf{E}}{\partial t} = \frac{\mathbf{E_{ij}^{n+1}} - \mathbf{E_{ij}^{n-1}}}{\mathbf{2\Delta t}} + O(\Delta t^2) \qquad (9)$$

where we omitted the subscript of the *y* – component of the electric field and where t= n Δt, x= k Δx, z= jΔz. Using an uniform grid (h= Δx = Δz), the method becomes

$$\begin{aligned}\mathbf{E}_{kj}^{n+1} = \frac{1}{1+s}\Bigg\{ \frac{1}{12} r^2 \Big[& -\mathbf{E}_{(k-2)j}^{n} + 16\mathbf{E}_{(k-1)j}^{n} + ... \\ & + 16\mathbf{E}_{(k+1)j}^{n} - \mathbf{E}_{(k+2)j}^{n} + ... \\ & - \mathbf{E}_{k(j-2)}^{n} + 16\mathbf{E}_{k(j-1)}^{n} + ... \\ & + 16\mathbf{E}_{k(j+1)}^{n} - \mathbf{E}_{k(j+2)}^{n} \Big] + ... \\ & + \left(2 - 5r^2\right)\mathbf{E}_{kj}^{n} + (s-1)\,\mathbf{E}_{kj}^{n-1} \Bigg\}\end{aligned} \qquad (10)$$

where

$$r = \frac{v\,\Delta t}{h}; \quad v = \frac{1}{\sqrt{\mu_0 \varepsilon}}; \quad s = \frac{\sigma}{\varepsilon}\frac{\Delta t}{2}$$

We show that the necessary stability condition is

$$r \leq \sqrt{\frac{3}{8}} \qquad (11)$$

which is the same as indicated by Alford et al. (1974) for the scalar wave-equation without damping (Appendix A).

To avoid numerical grid dispersion, we use spatial sampling of five points per wavelength.

The absorbing boundary conditions are implemented using the sheme of Cerjan et al. (1985) because of its simplicity and robustness.

We use the source function

$$f(t) = t^2 e^{-\alpha t} \sin(\omega_0 t)$$

where $\alpha = \frac{\omega_0}{\sqrt{3}}$; and f_0 is the central frequency and

$\omega_0 = 2\pi f_0$.

Examples

We tested our finite-difference modeling algorithm against actual data. This data where aquired in the granite mine DALVA 5 in the town of Rui Barbosa, state of Bahia, Brazil. The goal of the work was the correct mapping of the fractures in the granite. Here we face a typical situation: the excellent radar response of the granite was masked by a conductive clay overburden. The high conductivity (20mS/m) of this overburden attenuates strongly the radar response of subjacent structure and therefore makes the correct interpretation of the radargram more difficult. Then, forward modeling plays its role as a check to see if the interpretation is done correctly.

The real GPR section, shown in figure 1, was aquired along 43,2 m with a 200 MHz antenna and a GSSI SIR-2000 system. The processing of the actual data was: mute-off from t= 220 ns onwards, spectral analysis and application of a band-pass filter from 14 to 260 Mhz. Then we applied AGC gain with a time window of 40 ns and finally a filter with lateral correlation envolving 5 (five) traces.

The first model was built on geological observations, such as the large fractures in the granite quarry and its clay overburden, which were combined with the values of electrical permittivity and conductivity found in the literature (Davis and Annan, 1989). After several trial and error runs we obtained the geoelectric model shown in figure 2, where we used $\varepsilon_{air} = \varepsilon_0$, $\sigma_{air} = 0$, $\varepsilon_{clay} = 10\ \varepsilon_0$, $\sigma_{clay} = 20$ mS/m, $\varepsilon_{granite} = 4.6\ \varepsilon_0$, $\sigma_{granite} = 0.01$ mS/m and where the fracture in the granite is filled with the properties of air. Figure 3 is the syntetic zero-offset section using the central frequency of 200 MHz which corresponds to this model. Figure 4 is the same zero-offset section without considering attenuation, i.e. putting the conductivitiy to zero in the modeling algorithm. Finally, figure 5 is the

syntetic zero-offset section using the central frequency of 100 MHz which corresponds to the model shown in fig. 2.

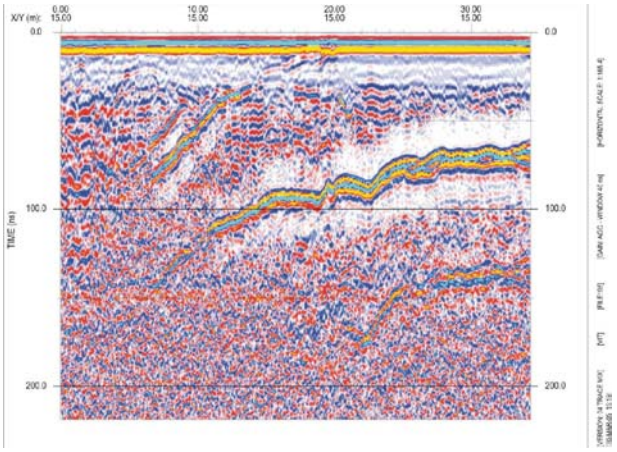

Figure 1: Real GPR section over the granite quarry, aquired along 43,2 m with a 200 MHz antenna and a GSSI SIR – 2000 System

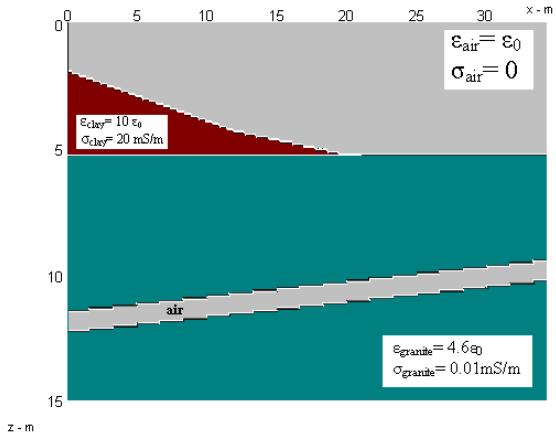

Figure 2: Geoelectric model of the granite quarry with a clay overburden where $\varepsilon_{air} = \varepsilon_0$, $\sigma_{air} = 0$, $\varepsilon_{clay} = 10\,\varepsilon_0$, $\sigma_{clay} = 20$ mS/m, $\varepsilon_{granite} = 4.6\,\varepsilon_0$, $\sigma_{granite} = 0.01$ mS/m and where the fracture in the granite is filled with the properties of air.

Results

Analyzing the figures, we clearly observe the good agreement between the real section shown in figure 1 and the syntetic section shown in figure 3. On the right portion of both sections we recognize the reflection of fracture in the granite quarry and its multiple reflection beneath. On the left portion of both sections we can see the effect of the attenuation caused by the clay overburden, masking

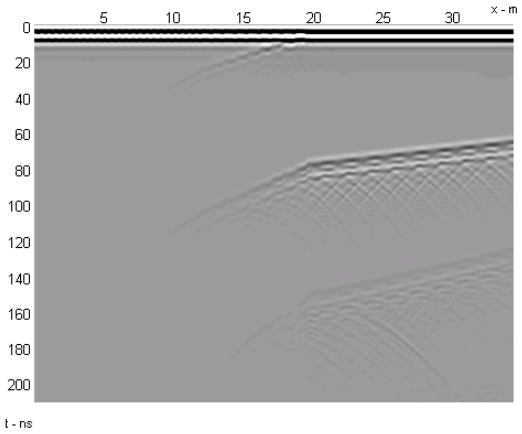

Figure 3: Syntetic zero-offset section of the geoelectric model shown in figure 2, computed with central frequency of 200 MHz and considering attenuation

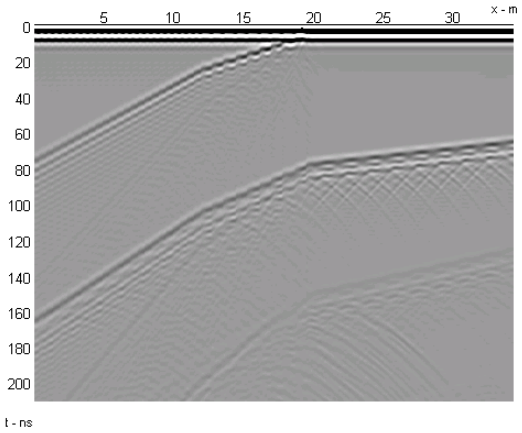

Figure 4: Syntetic zero-offset section of the geoelectric model shown in figure 2, computed with central frequency of 200 MHz and without attenuation

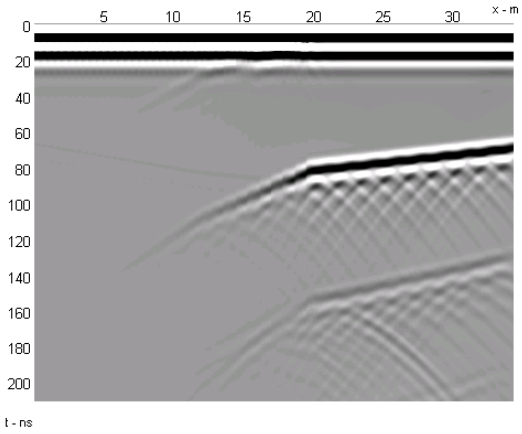

Figure 5: Syntetic zero-offset section of the geoelectric model shown in figure 2, computed with central frequency of 100 MHz and considering attenuation

the contact between the clay and the granite, as well as the fracture in the granite. The comparison of the syntetic section considering attenuation (fig. 3) with the syntetic section without attenuation (fig. 4) shows clearly the importance of the attenuation factor in our modeling tool to reproduce real GPR data. On the other side, simulations with zero conductivity as shown in fig. 4 are helpful to find an optimal geoelectric model. The comparison of the syntetic zero-offset section using the central frequency of 200 MHz (fig. 3) and the syntetic zero-offset section using the central frequency of 100 MHz (fig. 5) shows the increase of attenuation with the increase of frequency as discussed in the literature (e. g. Turner and Siggins, 1994).

Conclusions

In the present work we employ classical finite-differences to solve the damped scalar wave equation. We show that the stability condition for the damped scalar wave equation does not depend on the damping factor, being the same as the presented for the wave equation without attenuation presented by Alford et. al. (1974).

As an example application of our modeling tool we investigate a typical situation in granite prospecting, where a conductive clay masks the real position of the fractures in the granite. The results of the modeling have a good agreement with the actual data. Also, the algorithm shows well the increase in attenuation with the increase of the frequency.

The algorithm shows to be a good basic modeling tool.

Further work will be:

i) Use of the finite-difference algorithm in other practical applications for validating of actual data

ii) Comparison of the finite-difference algorithm with other direct modeling algorithms such as the pseudospectral method or the finite elements method

iii) Extension of the presented modeling algorithm to anisotropic and general frequency dependent media, such as treated by Carcione (1996)

Acknowledgments

We would like to thank CPGG/UFBA for logistical support. Also we thank ANP, Capes and CNPq for the financial support given to CPGG/UFBA.

References

Alford, R. M., Kelly, K. R., and Boore, D. M., 1974 Accuracy of finite-difference modeling of the acoustic wave equation: Geophysics, **39**, 834-842

Cai, J., and McMechan, G. A., 1995, Ray-based synthesis of bistatic ground-penetring radar profiles: Geophysics, **60**, 87-96

Carcione, J. M., 1996, Ground-penetrating radar: Wave theory and numerical simulation in lossy anisotropic media: Geophysics, **61**, 1664-1677

Casper, D. A., and Kung, K-J. S., 1996, Simulation of ground-petetrating radar waves in a 2-D soil model: Geophysics, **61**, 1034-1049

Cerjan, C., Kosloff, D., Kosloff, R., and Reshef, M., A, 1985, Nonreflecting boundary condition for discrete acoustic and elastic wave equations: Geophysics, **50**, 705-708

Chen, H-W., and Huang, T-M., 1996, Time-domain staggered-grid finite-difference simulation of GPR data: SEG Expanded Abstracts **15**, 796

Davis, J. L., and Annan, A. P., 1989, Ground-penetrating radar for high resolution mapping of soil and rock stratigraphy: Geophysical Prospecting, **37**, 531-551

Goodman, D., 1994, Ground-penetrating radar simulation in engineering and archaeology: Geophysics, **59**, 224-232

Thomas, J. W., 1995, Numerical Partial Differential Equations: Finite Difference Methods, Springer-Verlag New York, Inc.

Turner, G., and Siggins, A. F., 1994, Constant Q attenuation of subsurface radar pulses: Geophysics, **59**, 1192-1200

Zeng, X., McMechan, G. A., Cai, J., and Chen, H-W., 1995, Comparison of ray and Fourier methods for modeling monostatic ground-penetrating radar profiles: Geophysics, **60**,1727-1734

Appendix A

Derivation of the stability condition

We use a simplification of the von Neumann condition (e. g. Thomas, 1995). We consider

$$E_{kj}^{n} = \lambda^{n} e^{i\theta x_k} e^{i\psi z_j} \qquad (A.1)$$

and look for conditions that make $|\lambda| \leq 1$, which is the necessary condition for stability. Putting (A.1) in the finite difference method (10) yields, after some algebraic manipulation, the following quadratic equation for the amplification factor λ:

$$(s+1)\lambda^{n} + 2\alpha\lambda + (1-s) = 0 \qquad (A.2)$$

where

$$\alpha = \frac{r^2}{6}\left\{\left[\cos(\theta h) - 4\right]^2 + \left[\cos(\psi h) - 4\right]^2 - 18\right\} - 1$$

The solutions of (A.2) are

$$\lambda_{+} = \frac{-\alpha + \sqrt{\alpha^2 + s^2 - 1}}{1+s}$$

$$\lambda_{-} = \frac{-\alpha - \sqrt{\alpha^2 + s^2 - 1}}{1+s}$$

(i) If $\alpha > 1$, then $\alpha^2 + s^2 > 1$ and

$$\lambda_- < \frac{-1-\sqrt{1+s^2-1}}{1+s} = -1$$

what means that the method is unstable.

(ii) If $\alpha < -1$, then $\alpha^2 + s^2 > 1$ and

$$\lambda_+ > \frac{1+\sqrt{1+s^2-1}}{1+s} = 1$$

what means that the method is unstable.

(iii) If $\alpha^2 + s^2 < 1$, then $\lambda = \frac{-\alpha \pm i\sqrt{1-\alpha^2-s^2}}{1+s}$

and $|\lambda| = \frac{\sqrt{1-s^2}}{1+s} \leq 1$

(iv) If $\alpha^2 + s^2 \geq 1$ and $-1 \leq \alpha \leq 0$, then

$$0 = \frac{0+\sqrt{0}}{1+s} \leq \lambda_+ \leq \frac{1+\sqrt{1+s^2-1}}{1+s} = 1$$

$$-1 \leq \frac{0-\sqrt{1+s^2-1}}{1+s} \leq \lambda_- \leq \frac{1-\sqrt{0}}{1+s} \leq 1$$

(v) If $\alpha^2 + s^2 \geq 1$ and $0 \leq \alpha \leq 1$, then

$$-1 \leq \frac{-1+\sqrt{0}}{1+s} \leq \lambda_+ \leq \frac{0+\sqrt{1+s^2-1}}{1+s} \leq 1$$

$$-1 \leq \frac{-1-\sqrt{1+s^2-1}}{1+s} \leq \lambda_- \leq \frac{0+\sqrt{0}}{1+s} = 0$$

From (iv) and (v):

(vi) $\alpha^2 + s^2 \geq 1$ and $\alpha^2 \leq 1 \Rightarrow |\lambda| \leq 1$

From (iii) and (vi):

(vii) $\alpha^2 \leq 1 \Rightarrow |\lambda| \leq 1$

Therefore, the absolute value of the amplification factor is bounded by 1 if $|\alpha| \leq 1$ regardless of s. This means that the stability condition does not depend on s.

Thus, we have to impose the condition

$$-1 \leq \alpha \leq 1.$$

Considering that $\min(\alpha) = -1$, the equation

$$-1 \leq \alpha$$

is ever valid.

Considering that $\max(\alpha) = \frac{16}{3}r^2 - 1$, the equation

$$\alpha \leq 1$$

is valid for

$$r \leq \sqrt{\frac{3}{8}}$$

which is the same condition as given by Alford et. al. (1974) for the scalar wave equation without damping.